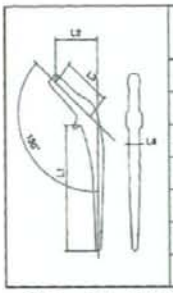

サイズ	ステム長 L1	オフセット幅 L2	ネック長 L3	近位部 A-P幅 L4
1号(SS・S・L)	94	27 / 32 / 37	27 / 34 / 41	9
2号(SS・S・L)	104	29 / 34 / 39	30 / 37 / 44	10
3号(SS・S・L)	113	31 / 36 / 41	32 / 39 / 46	11
4号(SS・S・L)	123	33 / 38 / 43	35 / 42 / 49	12
5号(SS・S・L)	127	33 / 38 / 43	35 / 42 / 49	13
6号(SS・S・L)	131	33 / 38 / 43	35 / 42 / 49	14
7号(SS・S・L)	140	35 / 40 / 45	37 / 44 / 51	16

図6　ステムサイズ（1～7号）

図7　ハイブリッド型THA 4 －U Hip System

図8 a

図8 b

図8　a術前のテンプレーティング（4 －U systemのNo. 1stem）　b術後

していた．

今回の解析結果より，

（1）ステム－セメントinterfaceはbondが望ましい．

（2）オフセットを一定にした場合，カラー下断面中心の外側水平方向5 mmまでの移動が生体力学的な許容範囲である．

という結論を得た．

日本人の骨格に適合した大腿骨ステムの設計

3次元有限要素法の解析結果を基に，ステムサイズ（1～7号）を決定した（図6）．1号ステムはCDH precoatステムより細く短い設計で，オフセットはCDHステムが22mmであるのに対し，1号ステムは32 mmと，10mm大きい設計となっている．この製品はハイブリッド型THA 4 －U Hip Systemとして，ナカシマメディカルより販売されている（図7）．

症　例

図1の症例では実際に4－U systemのNo.1stemを使用した（図8）．セメント使用ステムを用いる場合，欧米の製品では両者ともオフセットの小さいステム，あるいはカスタムメイドのステムを挿入せざるを得ないと思われる．各々術後5年,4年と短期ではあるが，疼痛の訴えはなく臨床成績は良好で，X線学的にも特に問題はない．

結　語

日本人の脱臼性および亜脱性股関節症患者73関節に対して大腿骨全長5mm間隔でCT撮影を施行し，結果を基にハイブリッド型人工股関節を開発した．ほぼ術前計画通り手術が行われ，現在のところその短期成績は良好である．

文　献

1）Ito H, Matsuno T, Minami A, et al. Intermediate-term results after hybrid total hip arthroplasty for the treatment of dysplastic hips. J Bone Joint Surg Am, 85 : 1725-1732, 2003.

2）Ito H, Matsuno T, Minami A. Pre-coated femoral components in hybrid total hip arthroplasty. Results at 11years. J Bone Joint Surg Br, 87 : 306-309, 2005.

3）Ito H, Hirayama T, Tanino H, et al. Tight fit technique in primary hybrid total hip arthroplasty for patients with hip dysplasia. J Arthroplasty,22 : 57-64, 2007.

4）Tanino H, Ito H, Higa M, et al. Three-dimensional computer-aided design based design sensitivity analysis and shape optimization of the stem using adaptive p-method, J Biomech, 39(10) : 1948-1953, 2006.

5）Tanino H, Ito H, Harman MK, et al. An in vivo model for intraoperative assessment of impingement and dislocation in total hip arthroplasty. J Arthroplasty, 23 : 714-720, 2008.

6）比嘉昌，西村生哉，谷野弘昌，ほか．人工股関節ステム形状の骨セメント内応力への影響，日本臨床バイオメカニクス学会誌，23：167－171，2002.

7）比嘉昌，西村生哉，谷野弘昌，ほか．p法有限要素解析による人工股関節ステムのデザイン感度解析．日本整形外科学会雑誌，74（8）：S1783，2000.

8）比嘉昌，西村生哉，谷野弘昌，ほか．人工股関節ステム形状の骨セメント内応力への影響．日本臨床バイオメカニクス学会誌，23：167－171，2002.

9）石田敏真，西村生哉，谷野弘昌，ほか．三次元有限要素法を用いた人工股関節ステム形状の最適設計．日本整形外科学会雑誌，77（8）：S1194，2003.

10）石田敏真，八木橋厚太，西村生哉，ほか．PERFECTA IMC stemの応力解析．日本臨床バイオメカニクス学会誌，26：233－237，2005.

11）石田敏真，西村生哉，三田村好矩，ほか．遺伝アルゴリズムを応用した人工股関節ステム形状の最適設計，生体医工学，46（2）：226－231，2008.

12）松田雄弘，西村生哉，谷野弘昌，ほか．三次元CADモデルを用いたアダプティブP法FEMによる全人工股関節ステム形状の最適設計．電子情報通信学会技術研究報告（MEとバイオサイバネティックス），101（130）：9－14，2001.

13）松野丈夫，伊藤浩，勇田敏夫，ほか．日本人の股関節骨格形態に適合した人工股関節の研究開発．ホクサイテック財団研究開発支援事業研究成果報告書：161－164，2000.

14）松野丈夫，谷野弘昌，大水信幸ほか：人工股関節置換術　弛むことのない人工関節への夢．旭川医科大学研究フォーラム，2（1）:30－35，2001.

15）中村聡喜，伊藤浩，谷野弘昌，ほか．THA後の可動域をより改善させるネック形状についての研究．日本整形外科学会雑誌，79（8）S790，2005.

16）中村聡喜（旭川医科大学整形），伊藤浩，谷野弘昌，ほか．THA後の日常生活動作を満たすネック形状と骨頭径についての研究．日本整形外科学会雑誌，80（8），S944，2006.

17）大水信幸，伊藤浩，谷野弘昌，ほか．セメントステム近位内側形状の応力環境への影響．日本整形外科学会雑誌，74（8）：S1784，2000.

18）谷野弘昌，伊藤浩，石田敏真，ほか．多目的最適化によるセメントステムデザインの検討．日本整形外科学会雑誌，79（8），S817，2005.

Tumor Location Affects the Results of Simple Excision for Multiple Osteochondromas in the Forearm

By Jun-ichi Ishikawa, MD, Hiroyuki Kato, MD, Fumio Fujioka, MD, Norimasa Iwasaki, MD, Naoki Suenaga, MD, and Akio Minami, MD

Investigation performed at the Department of Orthopaedic Surgery, Hokkaido University School of Medicine, Sapporo, Japan

Background: The effectiveness of excision of osteochondromas in controlling the progression of forearm and wrist deformity remains an issue of controversy. The purpose of this study was to analyze the effectiveness of tumor excision in the correction of forearm and wrist deformity due to multiple osteochondromas in children, with an interpretation of the results based on different patterns of deformity.

Methods: Fourteen forearms in thirteen children with a follow-up of more than twenty-four months (average, fifty-three months) were included in the study. The forearms were divided into two groups on the basis of the location of the tumor and the pattern of deformity. In Group 1 (six forearms), the osteochondroma was only in the distal aspect of the ulna and caused compression of the radius. In Group 2 (eight forearms), tumors were in both the distal aspect of the ulna and the ulnar side of the distal part of the radius and were in contact with each other. Radial length, ulnar shortening, radial bowing, the radial articular angle, and carpal slip were measured as radiographic parameters. Ulnar shortening and radial bowing were expressed as a percentage of the radial length to make it possible to compare data between the individuals. Each parameter was evaluated before surgery and at the time of final follow-up.

Results: In Group 1, the percentage of ulnar shortening and the percentage of radial bowing had improved at the time of final follow-up; however, in Group 2, both the radial articular angle and the percentage of radial bowing had deteriorated significantly after the tumor excision ($p = 0.049$ and $p = 0.017$, respectively), even though the percentage of ulnar shortening showed no change.

Conclusions: The effectiveness of simple excision of osteochondromas of the distal aspect of the forearm is influenced by the tumor location and is related to the pattern of the deformity. Simple tumor excision can correct the forearm deformity in patients with an isolated tumor of the distal part of the ulna. Conversely, in patients with tumors involving the distal part of the ulna and the ulnar side of the distal end of the radius, tumor excision alone is a less promising procedure for the correction of the deformity.

Level of Evidence: Prognostic Level IV. See Instructions to Authors for a complete description of levels of evidence.

Multiple osteochondromas frequently affect the distal aspects of the radius and ulna and can result in severe deformity of the wrist and forearm. Such deformity is caused by a combination of shortening of the ulna, bowing of the radius, and ulnar deviation of the wrist, and, occasionally, radial head dislocation[1]. Radial articular deformity in association with multiple osteochondromas (an increasing radial articular angle) may be induced by tethering of the shortened distal aspect of the ulna, as first proposed by Solomon in 1961[2], and subsequently supported by several other studies[3-5]. Solomon also theorized that relative ulnar shortening was accommodated by either bowing of the radius or dislocation of the radial head proximally. However, more recently Burgess and Cates performed a radiographic evaluation of a forearm deformity in thirty-five patients (sixty-five forearms) with multiple osteochondromas and showed that ulnar short-

Disclosure: The authors did not receive any outside funding or grants in support of their research for or preparation of this work. Neither they nor a member of their immediate families received payments or other benefits or a commitment or agreement to provide such benefits from a commercial entity. No commercial entity paid or directed, or agreed to pay or direct, any benefits to any research fund, foundation, division, center, clinical practice, or other charitable or nonprofit organization with which the authors, or a member of their immediate families, are affiliated or associated.

TABLE I Radiographic Data on All Patients Before the Operation and at the Time of the Final Follow-up

Case	Gender	Age at Time of Operation (*yr + mo*)	Side	Duration of Follow-up (*mo*)	Ulnar Shortening (%)		Radial Bowing (%)		Radial Articular Angle (*deg*)		Carpal Slip* (%)	
					Preop.	Final	Preop.	Final	Preop.	Final	Preop.	Final
Group 1												
1	F	5 + 2	R	25	7.7	8.4	6.9	6.2	29	28	100	83.3
2	F	9 + 2	R	48	8.9	6.5	13.1	11.0	42	41	52.2	58.3
3	F	6 + 3	L	77	6.7	2.9	7.6	3.9	26	26	53.8	45.5
4	F	4 + 1	L	27	15.2	11.8	13.0	8.1	28	28	–	–
5	F	12 + 3	R	24	2.5	1.9	10.3	8.8	38	36	75.0	57.1
6	M	4 + 5	L	97	9.0	7.4	10.4	5.8	20	21	–	–
Group 2												
7	M	6 + 2	L	46	9.3	8.3	9.3	9.4	42	63	90.0	111.8
8	M	14 + 6	R	24	0.3	0.3	6.2	7.9	47	41	93.3	70.6
			L	24	0.3	1.9	5.8	8.3	35	55	76.9	105.9
9	F	5 + 4	L	54	13.2	12.9	6.6	8.4	34	37	90.9	47.4
10	M	8 + 11	R	83	5.8	6.9	7.2	6.9	35	33	56.3	35.7
11	M	9 + 4	L	48	7.3	5.1	6.5	8.5	28	42	62.5	62.5
12	F	7 + 1	R	92	2.9	3.0	5.9	7.5	32	42	45.5	56.0
13	M	9 + 10	R	77	4.4	7.7	7.3	7.3	23	28	57.1	33.3

*Data on carpal slip in two patients (Cases 4 and 6) were excluded because of insufficient ossification of the lunate before the operation.

ening was not related to subsequent shortening of the radius or to distal radial deformity, providing evidence against the ulnar tether theory[6]. Alternatively, their results suggest that both the radius and the ulna exert proportional suppression of growth, and the loss of radial length is caused by involvement of the radius in the pathological process, and not by an ulnar tether. This speculative argument was supported by Ogden on the basis of a histological study of an osteochondroma in the fibula of a three-year-old girl, which showed that the osteochondroma invaded the epiphysis and had the potential to further invade the growth plate[7]. Masada et al. classified forearm deformities that were due to multiple osteochondromas and reported the outcome of several surgical procedures; these data showed that the bulk of osteochondromas themselves plays an important role in inducing radial bowing[8]. Therefore, forearm deformity may be the result of various etiologic factors associated with multiple osteochondromas (ulnar shortening, growth disturbance, and/or compression by the tumor itself).

Tumor excision is the most common surgical treatment, and this procedure can be combined with other surgical methods, including ulnar lengthening, radial osteotomy, and hemiepiphysiodesis, depending on the severity and pattern of the deformity[3,5,8-13]. However, the variety of combinations of surgical procedures has made it difficult to assess the effectiveness of each procedure for the correction of the deformity, leading to a long-standing controversy regarding the overall effectiveness of the excision of osteochondromas in controlling the progression of a deformity. Masada et al. suggested that a simple excision can prevent the progression of the disease and is effective in controlling radial bowing[8]; however, Fogel et al., in a study of simple excision in ten patients, found that early excision of the osteochondroma alone did not improve the wrist deformity, although the procedure did reduce the rate of progression of ulnar shortening compared with the preoperative rate[10].

The purpose of the current study was to investigate the effect of simple excision of osteochondroma(s) on the correction of the deformity, on the basis of the changes in radiographic parameters. Various patterns of deformity were classified radiographically according to the location of the tumor, and these were related to the etiologies of the deformity. We hypothesized that a forearm deformity can be defined by the tumor location and that the type of deformity influences the effectiveness of simple excision for the correction of the deformity.

Materials and Methods

Fifty-seven surgical procedures in twenty-five patients (thirty forearms) with multiple osteochondromas were performed in our department between 1983 and 2005. Excision of osteochondromas was performed in all patients. Accompanying procedures included ulnar lengthening (eighteen forearms), radial osteotomy (two forearms), and radial hemiepiphysiodesis (seven forearms). The ulnar lengthening was usually performed when the radial head was dislocated proximally in association with severe ulnar shortening, and radial osteotomy or radial hemiepiphysiodesis was performed when the lunate had slipped beyond the ulnar edge of the distal part of the radius with increased radial inclination of the distal end of the radius. The purpose of this study was to assess the effectiveness of tumor excision for the correction of a deformity; therefore, fourteen forearms in thirteen patients who had a

Fig. 1

Radiographic measurement of ulnar shortening (US), radial bowing (RB), carpal slip, radial length (RL), and radial articular angle (RAA) (see text). The percentage of ulnar shortening = US / RL × 100; the percentage of radial bowing = RB / RL × 100; and carpal slip = b / a × 100.

simple tumor excision as an isolated procedure and were followed for more than twenty-four months were included in the study (Table I). Informed consent was obtained preoperatively from the patients and parents on the basis of the surgical indication as determined at our institution, and the patients returned for follow-up evaluation postoperatively. The patients included six boys and seven girls. In one patient, tumors were excised from both forearms. The average age at the time of surgery was 7.9 years (range, four to fourteen years), and the operation was performed when the patients were less than ten years old, except for two children who had surgery when they were twelve and fourteen years old. The average follow-up period was fifty-three months (range, twenty-four to ninety-seven months).

The forearm and wrist deformity were evaluated with use of plain anteroposterior radiographs according to the method reported by Burgess and Cates (Fig. 1)[6]. In this method, a linear axis is determined by a line connecting the ulnar borders of the distal and proximal physeal plates of the radius. Ulnar shortening is measured as the distance between the intersection of a line drawn perpendicularly at the level of the distal end of the ulna to the linear axis and the ulnar border of the distal physeal plate of the radius; the percentage of ulnar shortening is then calculated by dividing ulnar shortening by the length of the linear axis of the ulna. The radial articular angle is the angle between the linear axis of the radius and a line drawn along the distal articular surface of the radius. Radial bowing is defined as the greatest distance from the radial diaphysis to the linear axis of the radius and is expressed as the percentage of radial bowing, which is determined by dividing the radial bowing by the length of the linear axis. Carpal slip is determined by measuring the distance between the extreme ulnar side of the lunate and a continuation of the linear axis of the ulna, with this distance expressed as a percentage of the total length of the lunate. The extreme ulnar side of the lunate is defined as the contact point of a line drawn parallel to the linear axis of the lunate. In two four-year-old patients (Cases 4 and 6), the lunate had not yet ossified and carpal slip was excluded from the evaluation.

Two patterns of deformity were defined on the basis of the location of the tumor. In the six forearms in Group 1, the osteochondroma was present only at the junction of the metaphysis and diaphysis of the distal aspect of the ulna, and it resulted in compression of the radius, which was mainly reflected in altered radial bowing (Figs. 2-A and 2-B). The deformity of the distal end of the radius in this group was usu-

ally minimal. In the eight forearms in Group 2, the tumors were present at both the distal end of the ulna and the ulnar side of the radius, and they were in contact with each other (Figs. 3-A and 3-B). The percentage of ulnar shortening and the percentage of radial bowing were less severe in Group 2 compared with Group 1. No patient in either group had dislocation of the radial head; however, one patient (Case 4) in Group 1 showed lateral subluxation of the radial head, with severe ulnar shortening.

Osteochondromas were excised completely under radiographic image control because there was no clearly identifiable border between the base of the tumor and the normal bone. Usually the normal bone was partly excised at the base of the tumor with great care taken to not injure the growth plate. In Group 1, the osteochondroma of the distal part of the ulna was approached between the extensor carpi ulnaris and the flexor carpi ulnaris. In Group 2, the osteochondroma of each bone was excised through two separate skin incisions in order to reduce the possibility of creating a synostosis between the distal end of the radius and the ulna after the excision[12]. The osteochondroma on the ulnar side of the distal part of the radius was exposed through a radiopalmar skin incision with detachment of the pronator quadratus from the radius.

We compared the groups in terms of the preoperative radiographic parameters using the Mann-Whitney test. To evaluate the effect of simple tumor excision on the correction of the deformity, the radiographic parameters before surgery and at the time of the final follow-up were compared with use of the paired t test and the groups were compared, with use of the Mann-Whitney test, with respect to the changes in each parameter after surgery. A p value of 0.05 was considered to be significant.

Fig. 2-A

Fig. 2-B

Figs. 2-A through 2-D Case 4. A four-year-old girl in Group 1 who had a deformity of the left forearm.
Figs. 2-A and 2-B Preoperative radiographs showing a tumor in the distal diaphysis of the ulna with compression of the radius. The percentage of ulnar shortening was 15.2%, the percentage of radial bowing was 13%, and the radial articular angle was 28°.

Results

Preoperative Findings

Preoperative and postoperative radiographic parameters are shown in Table I. Groups 1 and 2 were compared with respect to these parameters. The average percentage of ulnar shortening, percentage of radial bowing, radial articular angle, and percentage of carpal slip were 8.3%, 10.2%, 30.5°, and 70.3%, respectively, in Group 1 and 5.4%, 6.9%, 34.5°, and 71.6%, respectively, in Group 2. Before surgery, the percentage of ulnar shortening and percentage of radial bowing were more severe in Group 1. A significant difference was recognized in the percentage of radial bowing ($p = 0.010$). There were no apparent differences in radial articular angle or carpal slip between Groups 1 and 2.

Postoperative Findings

There were no significant differences between Groups 1 and 2 in terms of age at the time of surgery (average, 6.9 and 8.7 years, respectively) or length of follow-up (fifty and fifty-six months, respectively).

The average changes in the radiographic parameters for all thirteen patients from before surgery to the final follow-up

Fig. 2-C

Fig. 2-D

Fig. 2-C Radiograph made twelve months postoperatively showing substantial remodeling of the bowed radius. **Fig. 2-D** Radiograph made twenty-seven months postoperatively showing that, although ulnar shortening remained, the percentage of ulnar shortening had improved to 11.8%. Radial remodeling had proceeded further, and the percentage of radial bowing had improved to 8.1%. The radial articular angle was unchanged from the preoperative value of 28°.

Fig. 3-A

Fig. 3-B

Figs. 3-A and 3-B Case 7. A six-year-old boy in Group 2 who had a deformity of the left forearm. **Fig. 3-A** Radiograph showing osteochondromas in the metaphysis of the distal aspect of both the radius and ulna, which were in contact with each other. The percentage of ulnar shortening was 9.3%, the percentage of radial bowing was also 9.3%, the radial articular angle was 42°, and the amount of carpal slip was 90%. **Fig. 3-B** Radiograph made forty-six months postoperatively showing the percentage of ulnar shortening and radial bowing were unchanged (8.3% and 9.4%, respectively), but both the radial articular angle and the carpal slip had deteriorated to 63° and 111.8%, respectively. The tumors had recurred, and a growth disturbance of the ulnar side of the distal aspect of the radius was suspected.

were 6.7% to 6.1% of ulnar shortening, 32.8° to 37.2° in the radial articular angle, 8.3% to 7.7% of radial bowing, and 71.1% to 64% of carpal slip. With this small number of patients, none of these changes were significant.

Changes in Radiographic Parameters After Surgery

Ulnar Shortening (Fig. 4)

The average percentage of ulnar shortening improved from 8.3% before surgery to 6.5% at the time of the final follow-up in Group 1 ($p = 0.047$), whereas no change was detected, with the numbers studied, in Group 2 (5.4% to 5.8%, respectively). The difference between the two groups with respect to the average change in the percentage of ulnar shortening (−1.8% in Group 1 and +0.4% in Group 2) after surgery was significant ($p = 0.039$). In Group 1, improvement of >2% was obtained in three patients (Cases 2, 3, and 4) (Figs. 2-A through 2-D) and two patients (Cases 1 and 5) showed almost no change in the percentage of ulnar shortening. In contrast, one patient in Group 2 (Case 13) showed a deterioration in the percentage of ulnar shortening of >2%.

Radial Bowing (Fig. 5)

The mean percentage of radial bowing in Group 1 improved significantly from 10.2% before surgery to 7.3% at the time of

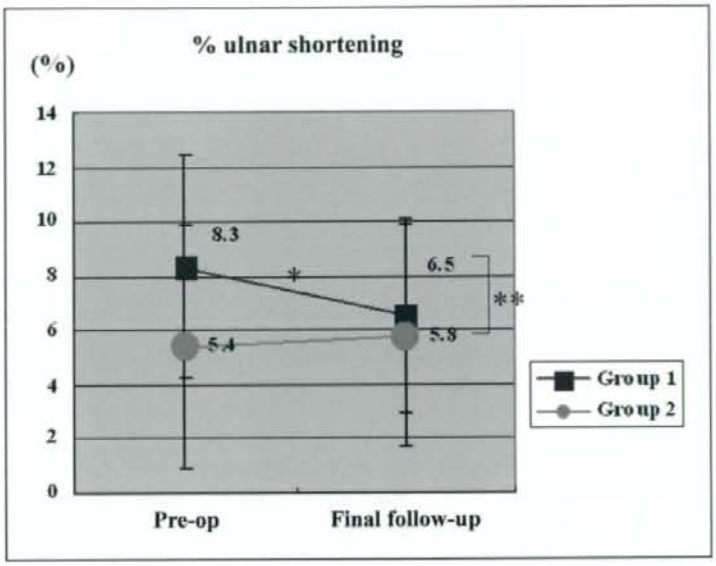

Fig. 4

Preoperatively, the average percentage of ulnar shortening was significantly more severe in Group 1 than in Group 2 (single asterisk; $p < 0.05$). At the time of the final follow-up, it had significantly improved to an average of 6.5% in Group 1 (single asterisk; $p < 0.05$), whereas there was no change in Group 2 (average, 5.8%). The difference in the postoperative change between the groups was significant (double asterisk; $p < 0.05$).

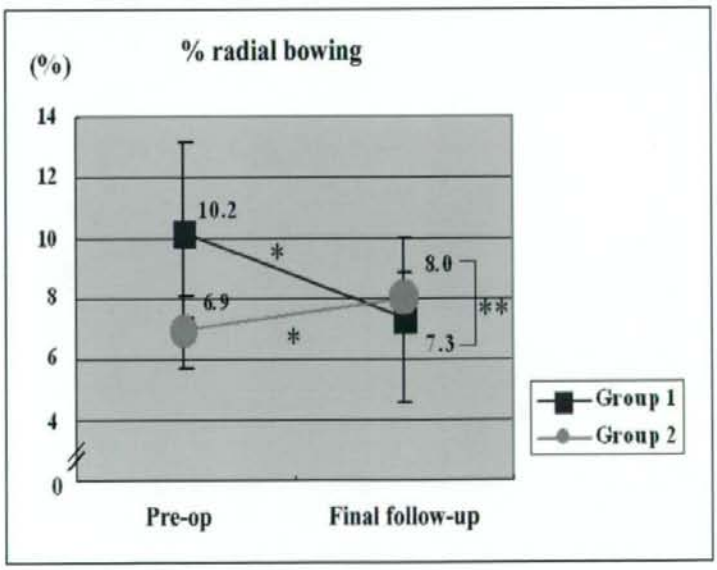

Fig. 5

Preoperatively, the average percentage of radial bowing was significantly more severe in Group 1 than in Group 2 ($p = 0.010$). At the time of final follow-up, it had significantly improved in Group 1, but had significantly deteriorated in Group 2 (single asterisk; $p < 0.05$ for both). The difference between the groups was significant (double asterisk, $p < 0.05$).

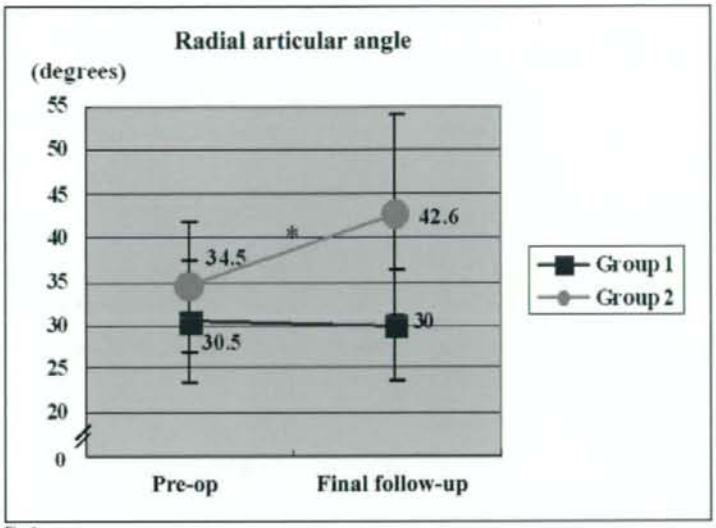

Fig. 6

At the time of final follow-up, the radial articular angle was unchanged in Group 1, but it had significantly deteriorated in Group 2 (asterisk; $p < 0.05$).

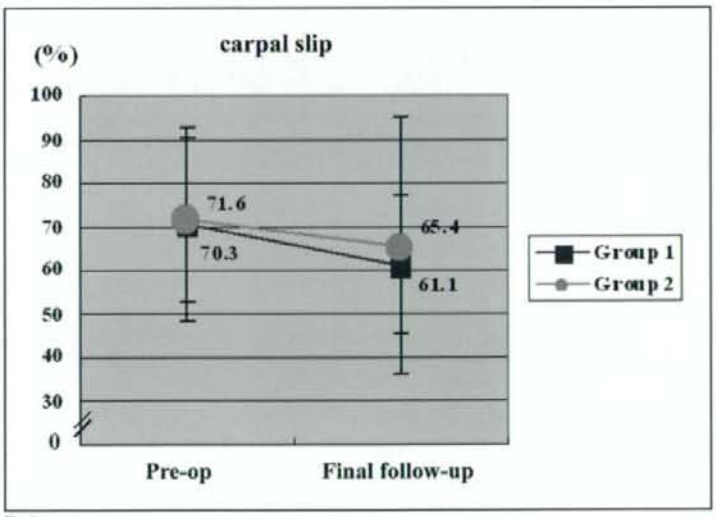

Fig. 7

The amount of preoperative carpal slip showed no significant change at the time of final follow-up.

the final follow-up ($p = 0.010$). Conversely, the mean percentage of radial bowing in Group 2 showed significant deterioration from 6.9% before surgery to 8.0% at the time of the final follow-up ($p = 0.017$). The difference between the groups with respect to the average change after surgery (−2.9% in Group 1 and +1.1% in Group 2) was also significant ($p = 0.002$).

Radial Articular Angle (Fig. 6)

At the time of the final follow-up, the mean radial articular angle had not changed in Group 1 (30.5° before surgery to 30.0° at the time of the final follow-up), but it had significantly deteriorated from 34.5° to 42.6° in Group 2 ($p = 0.049$). The difference between Groups 1 and 2 with respect to the

mean change after surgery (–0.5° and +8.1°, respectively) was not significant ($p = 0.106$). In four patients (Cases 7, 8, 11, and 12) in Group 2, the radial articular angle had increased by ≥10° at the time of final follow-up compared with the preoperative value.

Carpal Slip (Fig. 7)

The average carpal slip in Groups 1 and 2 was 70.3% and 71.6%, respectively, before surgery and 61.1% and 65.4%, respectively, at the time of the final follow-up. In both groups, the average carpal slip showed slight improvement; however, in two patients (Cases 7 and 8) in Group 2, carpal slip increased severely and reached values of >100% with accompanying increases in the radial articular angle at the time of the final follow-up (Fig. 3-B).

Recurrence of the Tumor

Some degree of tumor recurrence was recognized on the distal aspect of both the ulna and the radius in five patients (Cases 7 and 8 and, on the left side, in Cases 10, 12, and 13) in Group 2 and on the distal aspect of the ulna in two patients (Cases 2 and 6) in Group 1 at the time of the final follow-up. Recurrence was more frequent in the patients with the longer follow-up period. However, there were no clear differences in the radiographic parameters after surgery between the patients with and those without tumor recurrence in either group.

Discussion

In our patients with osteochondromas of the distal aspect of the forearm, the pattern of deformity differed according to the location of the tumor. In Group 1 (with the tumor in the metaphyseal-diaphyseal area and located far from the growth plate of the ulna), the percentage of ulnar shortening and the percentage of radial bowing were worse than those in Group 2, leading to compression of the radius. Radial bowing in the patients in Group 1 was, therefore, thought to be partly due to compression of the radius caused by the tumor, as well as to relative ulnar shortening[4]. The radial articular angle was usually minimal in the patients in Group 1, although ulnar shortening was severe; this is inconsistent with the ulnar tether theory and in agreement with the conclusions of Burgess and Cates[6]. Simple excision of the tumor resulted in improvement in the relative amounts of ulnar shortening and radial bowing in Group 1, indicating that radial bowing can be expected to correct by normal remodeling of the bowed radius, as well as through recovery of the ulnar growth rate after removal of the tumor, especially in younger patients with a greater potential for remodeling. In Group 1, there appeared to be little tethering effect between the distal aspects of the ulna and the radius; therefore, simple tumor excision should be enough to correct the forearm deformity when there is no dislocation of the radial head proximally.

The percentage of ulnar shortening in the patients in Group 2 was less severe than that in Group 1, which may reflect a growth disturbance of the distal aspect of the radius due to involvement by the tumor. Burgess and Cates described two patients with an increased radial articular angle in conjunction with positive ulnar variance[6], in whom the radiographic findings showed the tumor to be on the ulnar side of the distal part of the radius. Masada et al. classified forearm deformity according to the location of the osteochondromas[8]. In that classification system, Type-III deformities are those in which the tumor is in the distal aspect of the radius and is accompanied by relative radial shortening.

The effectiveness of different surgical approaches to correct a forearm deformity due to multiple osteochondromas was reported by Fogel et al.[10] and included the interesting case of a patient who had the same type of deformity as those in Group 2 in our study; that is, the tumors were on both the ulnar side of the distal aspect of the radius and the distal part of the ulna and were in contact with each other. After observation of that patient for eight years, the deformity of the wrist had progressed and radial hemiepiphysiodesis was performed to correct the deformity by retarding growth on the radial side of the distal part of the radius[10]. However, this procedure also resulted in a difference in forearm length of 2.3 cm compared with the contralateral forearm. In contrast to the findings in that patient, Wood et al. stated that if an osteochondroma is located on the radius, or if osteochondromas from both the radius and the ulna push against each other, only minimal deformity occurs[3].

In the current study, the percentage of ulnar shortening and the percentage of radial bowing were less severe in the patients in Group 2 than in those in Group 1, which is consistent with the findings of Wood et al.[3]. However, we suspect that the ulnar aspect of the distal part of the radius is more susceptible to growth disturbance compared with other parts of the radius. When tumors are on both the ulnar side of the distal part of the radius and the distal aspect of the shortened ulna and are in contact with each other, a tethering effect between the tumors might occur in a longitudinal direction and result in an increasing radial articular angle and radial bowing with the passage of time because of a growth disturbance of the ulnar side of the distal aspect of the radius. Solomon described a reason for the valgus deformity of the distal part of the tibia when osteochondromas develop in both the distal part of the tibia and the distal aspect of the fibula[2]. He concluded that the valgus deformity was caused by a tethering effect of the shortened fibula and not by uneven growth of the tibial physis because the distal tibial physis remained in its normal horizontal orientation. However, in our patients in Group 2, the distal radial physis showed ulnar tilting (Fig. 3-B), which suggests a growth disturbance of the ulnar side of the distal radial physis.

In our study, simple excision of the tumor was unable to correct the deformity in the patients in Group 2, and the radial articular angle and the percentage of radial bowing showed significant increases. It is difficult to conclude whether simple tumor excision in the patients in Group 2 was effective for the correction of the deformity because of the high recurrence rate of the tumor in five of the eight forearms. Such recurrence of the tumor after excision has been

reported to be frequent. Shin et al., in a study involving twenty-two patients managed with simple excision of osteochondromas, noted that the recurrence rate was 53.8% in patients who were less than ten years old[13]. We think that the tethering effect and the growth disturbance of the affected portions persisted even after tumor excision irrespective of tumor recurrence in Group 2. This resulted in the deterioration of the radial articular angle and radial bowing. Actually, the percentage of radial bowing in three patients (Cases 8 [right side], 9, and 11) and the radial articular angle in one patient (Case 11) deteriorated, although there was no recurrence of the tumor. We recommend ulnar lengthening to completely release the tethering and to support the ulnar carpus when the radial articular angle and carpal slip are severe in patients with a Group-2 type of deformity.

In conclusion, the pattern of forearm deformity can be classified on the basis of the location of the tumor. This pattern is determined by the absence (Group 1) or presence (Group 2) of the tethering effect between the ulnar side of the distal aspect of the radius and the distal end of the ulna, and the ability of simple surgical excision of the tumor to correct deformity is influenced by this pattern of deformity. We note that the number of patients in the current study was small, and a more extensive study is necessary to confirm these conclusions. ■

Jun-ichi Ishikawa, MD
Norimasa Iwasaki, MD
Naoki Suenaga, MD
Akio Minami, MD
Department of Orthopaedic Surgery, Hokkaido University School of Medicine, Kita-15, Nishi-7, Kita-ku, Sapporo 060-8638, Japan. E-mail address for J. Ishikawa: ishijet77@yahoo.co.jp

Hiroyuki Kato, MD
Department of Orthopaedic Surgery, Shinshu University School of Medicine, 3-1-1 Asahi, Matsumoto, Nagano 390-8621, Japan

Fumio Fujioka, MD
Department of Orthopaedic Surgery, Nagano Prefectural Children's Hospital, 3100 Toyoshina, Azumino, Nagano 399-8288, Japan

References

1. Solomon L. Hereditary multiple exostosis. J Bone Joint Surg Br. 1963;45:292-304.

2. Solomon L. Bone growth in diaphysial aclasis. J Bone Joint Surg Br. 1961;43:700-16.

3. Pritchett JW. Lengthening the ulna in patients with hereditary multiple exostoses. J Bone Joint Surg Br. 1986;68:561-5.

4. Siffert RS, Levy RN. Correction of wrist deformity in diaphyseal aclasis by stapling. Report of a case. J Bone Joint Surg Am. 1965;47:1378-80.

5. Wood VE, Sauser D, Mudge D. The treatment of hereditary multiple exostosis of the upper extremity. J Hand Surg [Am]. 1985;10:505-13.

6. Burgess RC, Cates H. Deformities of the forearm in patients who have multiple cartilaginous exostosis. J Bone Joint Surg Am. 1993;75:13-8.

7. Ogden JA. Multiple hereditary osteochondromata. Report of an early case. Clin Orthop Relat Res. 1976;116:48-60.

8. Masada K, Tsuyuguchi Y, Kawai H, Kawabata H, Noguchi K, Ono K. Operations for forearm deformity caused by multiple osteochondromas. J Bone Joint Surg Br. 1989;71:24-9.

9. Ip D, Li YH, Chow W, Leong JC. Reconstruction of forearm deformities in multiple cartilaginous exostoses. J Pediatr Orthop B. 2003;12:17-21.

10. Fogel GR, McElfresh EC, Peterson HA, Wicklund PT. Management of deformities of the forearm in multiple hereditary osteochondromas. J Bone Joint Surg Am. 1984;66:670-80.

11. Jiya TU, Pruijs JE, van der Eijken JW. Surgical treatment of wrist deformity in hereditary multiple exostosis. Acta Orthop Belg. 1997;63:256-61.

12. Peterson HA. Deformities and problems of the forearm in children with multiple hereditary osteochondromata. J Pediatr Orthop. 1994;14:92-100.

13. Shin EK, Jones NF, Lawrence JF. Treatment of multiple hereditary osteochondromas of the forearm in children: a study of surgical procedures. J Bone Joint Surg Br. 2006;88:255-60.

Osteoarthritis and Cartilage (2008) **16**, 772–778

doi:10.1016/j.joca.2007.11.004

Osteoarthritis and Cartilage

International Cartilage Repair Society

OARSI OSTEOARTHRITIS RESEARCH SOCIETY INTERNATIONAL

Alteration of *N*-glycans related to articular cartilage deterioration after anterior cruciate ligament transection in rabbits[1]

T. Matsuhashi M.D.†, N. Iwasaki M.D., Ph.D., Associate Professor†*, H. Nakagawa Ph.D., Associate Professor‡, M. Hato‡, M. Kurogochi Ph.D.‡, T. Majima M.D., Ph.D., Associate Professor†, A. Minami M.D., Ph.D., Professor† and S.-I. Nishimura Ph.D., Professor‡

† *Department of Orthopaedic Surgery, Hokkaido University Graduate School of Medicine, Sapporo, Japan*

‡ *Graduate School of Advanced Life Science, Frontier Research Center for Post-Genome Science and Technology, Hokkaido University, Sapporo, Japan*

Summary

Objective: Osteoarthritis (OA) is the most common of all joint diseases, but the molecular basis of its onset and progression is controversial. Several studies have shown that modifications of *N*-glycans contribute to pathogenesis. However, little attention has been paid to *N*-glycan modifications seen in articular cartilage. The goal of this study was to identify disease specific *N*-glycan expression profiles in degenerated cartilage in a rabbit OA model induced by anterior cruciate ligament transection (ACLT).

Methods: Cartilage samples were harvested at 7, 10, 14, and 28 days after ACLT and assessed for cartilage degeneration and alteration in *N*-glycans. *N*-Glycans from cartilage were analyzed by high performance liquid chromatography and mass spectrometry.

Results: Histological analysis showed that osteoarthritic changes in cartilage occurred 10 days after ACLT. Apparent alterations in the *N*-glycan peak pattern in cartilage samples were observed 7 days after ACLT, and overall *N*-glycan changes in OA reflected alterations in both sialylation and fucosylation. These changes apparently preceded histological changes in cartilage.

Conclusion: These results indicate that changes in the expression of *N*-glycans are correlated with OA in an animal model. Understanding mechanisms underlying changes in *N*-glycans seen in OA may be of therapeutic value in treating cartilage deterioration.

Key words: Cartilage, Osteoarthritis, *N*-Glycan.

Introduction

Chondrocyte metabolism is controlled by genetic and environmental factors, such as extracellular matrix (ECM) composition, soluble mediators, or mechanical factors[1,2]. Osteoarthritis (OA), which results from a breakdown in the balance of these factors, is the most common joint disease. To date, numerous studies have investigated its pathogenesis[1–8]. However, factors mediating onset and aggravation of OA are still controversial.

Glycobiology, defined as the analysis of biological function of sugar chains covalently bound to proteins and lipids, has been recently applied to molecular-based investigations[9]. Sugar chains attached to proteins (glycoproteins) and lipids (glycolipids) are commonly referred to as glycans. Glycoprotein glycans are found on the cell surface, in the ECM, and in serum. These glycans act as an interface on the cell surface and modulate protein properties, including folding, secretion, targeting, and protease resistance[10,11]. Several studies show that glycan modifications of proteins contribute to the pathogenesis of some diseases[12,13]. One characteristic of cartilage is that some chondrocytes reside in areas rich in ECM. In addition, it is well known that glycoproteins are abundant on the cell surface and in cartilage ECM. These observations lead to a working hypothesis that sugars attached to proteins contribute to chondrocyte metabolism.

Glycans attached to proteins are classified into two groups: glycans attached to an asparagine residue through a nitrogen atom (*N*-glycans) and those attached to a serine or threonine oxygen (*O*-glycans)[11]. Both types have been intensively studied, and many studies report structural and functional analyses of *N*-glycans[14]. Based on these data, a relationship between *N*-glycan alteration and disease has recently been emerged[12,13,15–18]. For example, several studies of *N*-glycans of serum immunoglobulin G (IgG) molecules associated with the rheumatoid arthritis (RA) indicate that changing *N*-glycan structure contributes to RA[19–21]. However, little attention has been paid to *N*-glycan alterations occurring in articular cartilage in a diseased condition.

Glycans have five major functions: (1) providing cell wall and ECM structural components, (2) modifying protein

[1]Supported by a grant for the National Project on "Functional Glycoconjugate Research Aimed at Developing New Industry" from the Ministry of Education, Science, Sport and Culture of Japan, and SENTAN from the Japan Science and Technology Agency and Uehara Memorial Foundation.

*Address correspondence and reprint requests to: Dr Norimasa Iwasaki, Department of Orthopaedic Surgery, Hokkaido University Graduate School of Medicine, 060-8638, North 15, West 7, Kita-ku, Sapporo, Hokkaido, Japan. Tel: 81-11-706-5936 ext. 5937; Fax: 81-11-706-6054; E-mail: niwasaki@med.hokudai.ac.jp

Received 11 November 2006; revision accepted 17 November 2007.

properties, (3) directing glycoconjugates, (4) mediating and modulating cell adhesion, and (5) mediating and modulating signaling. Thus, we hypothesized that cartilage *N*-glycans would be altered in parallel with cartilage degradation in OA and would vary according to the degree of deterioration. Particularly, *N*-glycan alterations should occur at early phases of OA aggravation. To test this hypothesis, we analyzed *N*-Glycans of rabbit OA cartilage explants induced by anterior cruciate ligament transection (ACLT). The specific aims of this study were to clarify the alterations in cartilage *N*-glycans with OA aggravation and to identify *N*-glycan structures correlated with cartilage deterioration.

Materials and methods

ANIMALS AND SURGICAL PROCEDURES

Seventy-eight adult female Japanese white rabbits (15–16-week-old) weighing 2.6–3.1 kg purchased from a professional breeder (Japan SLC, Inc., Hamamatsu, Japan) were used for this study according to the established ethical guidelines approved by the local animal care committee. Rabbits were anesthetized with 0.6 ml pentobarbital sodium (50 mg/ml) injections and then maintained on isoflurane. To induce osteoarthritic changes of articular cartilage, the right knee ACL was sectioned through a medial parapatellar incision (OA group). As a sham control, arthrotomy without ACLT was performed in sham group. Rabbits were housed in plastic cages and allowed to move freely after the operation. At days 0, 7, 10, 14, and 28, animals were euthanized by an intravenous injection of overdose pentobarbital to obtain cartilage samples for histological and glycostructural analyses. Serum samples were harvested prior to euthanasia. Here, day 7 is defined as 7 days after the operation, and day 0 means the day prior to the operation.

HISTOLOGICAL ANALYSIS ($N = 36$)

To determine osteoarthritic changes in OA and sham groups, cartilage samples ($n = 4$) were analyzed histologically at days 0, 7, 10, 14, and 28. Each sample, including the tibial plateau and femoral condyle, was fixed in 10% neutral buffered formalin. Tissue blocks were decalcified with 14% ethylenediaminetetraacetic acid (EDTA), cut in a sagittal plane, and stained with hematoxylin and eosin (HE) and Safranin O–fast green. To avoid observer bias, slides were coded prior to microscopic analysis. Osteoarthritic changes in each sample were quantified using the modified Mankin score[22].

PREPARATION OF PYRIDYLAMINATED (PA)-*N*-GLYCAN ($N = 42$)

Cartilage samples of the tibial plateau and serum were obtained from each animal at days 0, 7, 10, and 28. Cartilage minced by a razor and serum was heated to 90°C for 15 min. After lyophilization, each sample was digested sequentially with trypsin, chymotrypsin, *N*-glycosidase F, and pronase as described[23]. *N*-Glycan fractions were purified on a gel-filtration column (Bio-Gel P-4, 1 × 38 cm, water, Nippon Bio-Rad Laboratories KK, Tokyo, Japan), and tagged by fluorescent labeling using 2-aminopyridine to increase sensitivity for analysis[24]. Excess reagents were removed by gel-filtration on Sephadex-G-15 (Amersham Bioscience, Tokyo, Japan). PA-*N*-glycans were analyzed using high performance liquid chromatography (HPLC) and mass spectrometry (MS).

HPLC ANALYSIS

HPLC analysis using the L-7000 HPLC system (Hitachi High-Technologies, Tokyo, Japan) was performed under conditions previously described[25,34,36]. PA-*N*-glycans were separated on an octadecylsilica (ODS) column (HRC-ODS, 6 × 150 mm, Shimadzu, Kyoto, Japan), and each peak on the ODS column was applied individually to an amide column (TSK-gel Amide-80, 4.6 × 250 mm, Tosoh, Tokyo, Japan). The relative amount of PA-*N*-glycans was calculated based on the peak area analyzed by attached software on the HPLC system. Elution positions of PA-*N*-glycan on the ODS and amide columns were converted to glucose units (GU), which corresponded to relative degree of polymerization of α1,6-glucose oligosaccharides, for increasing reproducibility. *N*-Glycan structures were suggested by comparing elution positions with data reported in the same analytical conditions, and confirmed with further HPLC analysis combined with partial digestion, and/or MS. Elution positions and code numbers of approximately 500 kinds of oligosaccharide are described in these references[34,35]. The validity of the elution positions and partial digestions was confirmed using well-known standard PA-*N*-glycans and previous studies[27,36].

N-Glycans can form various structures, but have a common core structure and some rules in linkages[11]. To determine the detailed *N*-glycans' structure related to OA, PA-*N*-glycans were digested sequentially with β-*N*-acetylhexosaminidase (HexNAcase, Jack bean, Seikagaku Co., Tokyo, Japan) which removed β-linked GalNAc and GlcNAc, α1,3/4-fucosidase (α3/4-Fase, Takara Co., Shiga, Japan) and weak hydrochloric acid to hydrolyze sialic acids. After each digestion, PA-*N*-glycans were individually analyzed by HPLC on both columns to confirm elution positions[23,25].

MS

To identify the PA-*N*-glycan structure, some PA-*N*-glycans separated by HPLC were further analyzed by matrix-assisted laser desorption/ionization time-of-flight MS (MALDI-TOF MS) using an Ultraflex TOF/TOF mass spectrometer (Bruker Daltonics GmbH, Bremen, Germany). As matrices, 2,5-dehydroxybenzoic acid (DHB) and α-cyano-4-hydroxycinnaminic acid (CHCA) were used. PA-*N*-glycans fractionated on HPLC were dissolved and applied to MALDI-TOF MS as described[26]. Based on results from HPLC and MS, each precise *N*-glycan structure was determined.

All measurements were performed using an Ultraflex TOF/TOF mass spectrometer equipped with a reflector and controlled by the FlexControl 2.2 software package (Bruker Daltonics). In MALDI-TOF MS reflector mode, ions generated by a pulsed UV laser beam (nitrogen laser, $\lambda = 337$ nm, 5 Hz) were accelerated to a kinetic energy of 23.5 kV. Metastable ions generated by laser-induced decomposition of the selected precursor ions were analyzed without any additional collision gas. In MALDI-LIFT-TOF/TOF mode, precursor ions were accelerated to 8 kV and selected in a timed ion gate. The fragments were further accelerated by 19 kV in the LIFT cell (LIFT indicates "lifting" the potential energy for the second acceleration of ion source), and their masses were analyzed after the ion reflector passage. Masses were automatically annotated by using the FlexAnalysis 2.2 software package. External calibration of MALDI mass spectra was carried out using singly charged monoisotopic peaks of a peptide mixture of human angiotensin II (*m/z* 1046.542), bombesin (*m/z* 1619.823), ACTH-(18–39) (*m/z* 2465.199), and somatostatin 28 (*m/z* 3147.472).

STATISTICAL ANALYSIS

Data were represented as means ± standard deviation (SD). Significant differences between groups were assessed by unpaired *t* tests. *P*-values of less than 0.05 were considered significant.

Results

HISTOLOGICAL FINDINGS

After the operations, rabbits exhibited a normal gait pattern by footprint analysis (data not shown). Also, infections were not seen macroscopically in any knee joint (data not shown). At day 7, no histological changes of the tibial plateau were seen in HE-stained samples of the OA group [Fig. 1(b)]. Samples evaluated at day 10 showed common OA changes, including deterioration of the superficial cartilage layer and a reduced number of chondrocytes in superficial and middle cartilage layers [Fig. 1(c)]. At day 28, a reduced number of chondrocytes were observed in whole layers [Fig. 1(e)], and cloning of chondrocytes was apparent in these damaged areas [Fig. 1(e)]. While Safranin O–fast green staining showed no significant change from day 7 to day 14 [Fig. 1(g–i)], both showed significant reduction at day 28 [Fig. 1(j)]. In the sham group, from day 7 to day 28 no histological indications of OA changes were observed in any samples (data not shown). Histological changes of the femoral condyle were observed later than histological changes of the tibial plateau (data not shown). After day 10, mean histological scores of the tibial plateau were significantly higher in the OA group than in the sham group (3.6 ± 0.5 vs 2.3 ± 0.5 at day 10, $P < 0.05$; 7.0 ± 0.6 vs 2.4 ± 0.4 at day 28, $P < 0.05$, Fig. 2).

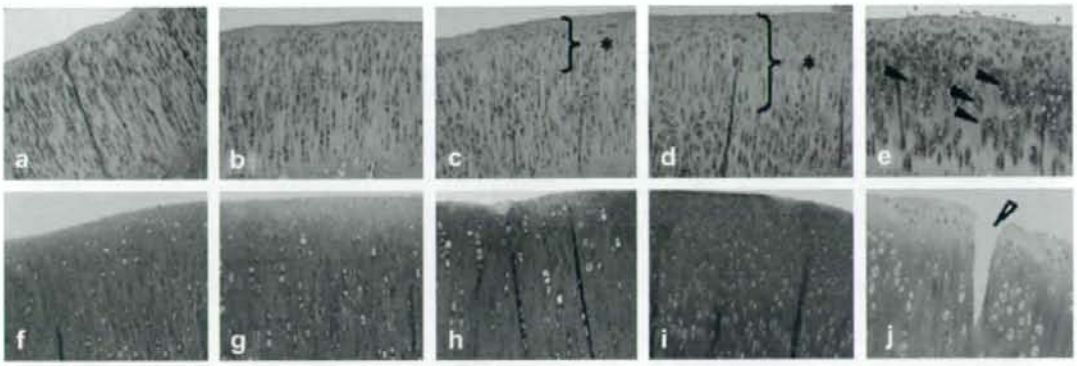

Fig. 1. Histology of cartilage after ACLT in medial tibial plateau in the rabbit knee joint. (a–e) HE-stained sections. (f–j) Safranin O-fast green stained sections. (a) Control articular cartilage shows a smooth surface. (b) At day 7, no significant changes compared with control cartilage were observed. (c) At day 10, superficial diffuse loss of chondrocytes (*) with surface irregularity was observed. (d) At day 14, diffuse loss of chondrocytes from superficial and middle zones (*) with surface irregularity was observed. (e) At day 28, diffuse loss of chondrocytes in the whole zone with clone formation (solid arrow) was observed. (f) Control articular cartilage with Safranin O-fast green stain. (g–i) At days 7,10, and14, no significant change of Safranin O-fast green staining was observed. (j) At day 28, severe loss of Safranin O–fast green staining and clefts (empty arrow) was observed.

ALTERATION IN *N*-GLYCAN PROFILES

We found no significant alterations in the *N*-glycan peak pattern of serum from day 7 to day 28 in the OA group (Fig. 3). In cartilage analysis, there were no apparent alterations in the *N*-glycan peak pattern from day 7 to day 28 in the sham group. By contrast, significant alterations in the *N*-glycan peak pattern in cartilage were observed in the OA group from day 7 postoperatively (Fig. 4). Alterations in peak shape suggested a change in the composition of *N*-glycans contained in the peak. To confirm this, we purified peaks by HPLC on an ODS column and analyzed each on an amide column in a different chromatographic mode. Each altered peak on the ODS column was separated into three peaks on the amide column, referred to as *N*-glycan A (a), B (b), and C (c) in the order of separation time (Fig. 4*). We then calculated each area ratio. The mean ratio of *N*-glycan A in the OA group significantly decreased from day 7 to day 28 compared to the sham group (40.6 ± 1.80 vs 36.0 ± 1.40 at day 7, $P < 0.05$; 39.8 ± 1.54 vs 35.6 ± 1.97 at day 28, $P < 0.05$, Fig. 5), while the value of *N*-glycan C in the OA group significantly increased from day 7 compared to the sham group (44.7 ± 1.91 vs 40.8 ± 1.28 at day 7, $P < 0.05$; 46.0 ± 2.67 vs 40.2 ± 1.03 at day 28, $P < 0.05$, Fig. 5). The mean ratio of *N*-glycan B did not significantly change (data not shown). The mean ratio of *N*-glycans A–C after day 7 was significantly higher in the OA group than in the sham group (1.25 ± 0.11 vs 1.01 ± 0.04 at day 7, $P < 0.05$; 1.32 ± 0.11 vs 1.01 ± 0.04 at day 28, $P < 0.05$, Fig. 5).

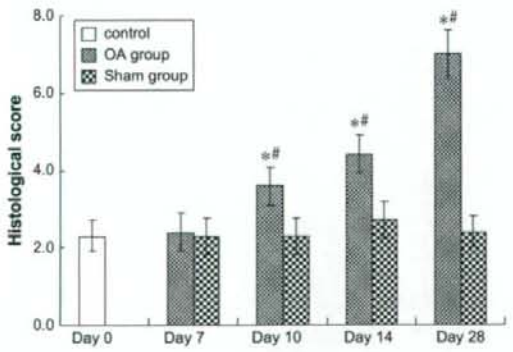

Fig. 2. Histological scores of medial tibial plateau. Values are means ± SD. Shown are scores for histological parameters with comparisons between groups. Histological analysis revealed that slightly degenerative changes in cartilage occurred in all cases starting 10 days after ACLT. *Denotes statistical significance ($P < 0.05$) vs sham group. #Denotes statistical significance ($P < 0.05$) vs control.

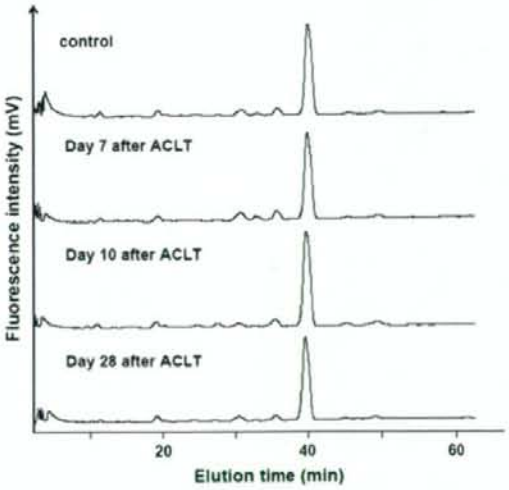

Fig. 3. Chromatograms of PA-*N*-glycans obtained from rabbit serum glycoproteins on an ODS column. There were no significant alterations in the *N*-glycan peak pattern of serum from day 7 to day 28 in the OA group compared with controls.

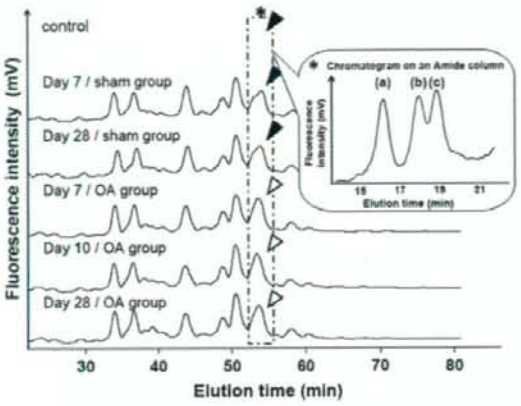

Fig. 4. Chromatograms of PA-*N*-glycans obtained from rabbit cartilage glycoproteins on an ODS column. Two peaks (solid arrow) in the chart of day 0 and the sham-operated group were seen as one peak (empty arrow) from day 7 after ACLT. Those peaks included three peaks on an amide column, referred to as *N*-glycan A (a), B (b), and C (c), in the order of separation time (*).

STRUCTURAL ANALYSIS OF *N*-GLYCANS RELATED TO OSTEOARTHRITIC CHANGES

MALDI-TOF spectra of *N*-glycans A and C with DHB as a matrix indicated a molecular mass of 2239.6 and 2094.6, respectively (Fig. 6). Each MALDI-TOF/TOF spectra showed constituents of *N*-glycans A and C (Fig. 7). MALDI-TOF and TOF/TOF spectra of *N*-glycans with CHCA as a different matrix indicated almost the same mass fragmentation compared with DHB (data not shown). Molecular mass of 2239.6 and 2094.6 corresponds with a protonated PA-glycan which consists of 3 Hex, 6 HexNAc and *N*-acetylneuraminic acid (NANA); and 3 Hex, 6 HexNAc and Fuc, respectively. These compositions and abundant fragment peaks of di-HexNAc (406.9 and 407.1) and peaks devoid of di-HexNAc, 1542.1 and 1542.2, indicate these *N*-glycans which include GalNAc–GlcNAc units instead of Gal–GlcNAc units in their outer arms. After sequential partial digestion, elution positions of both *N*-glycans on the two-dimensional map coincided with 110.4a GalNAcβ1,4-GlcNAcβ1,2-Manα1,3-(Manα1,6-)Manβ1,4-GlcNAcβ1,4-(Fucα1,6-)GlcNAc which confirmed from a previous study combining HPLC, NMR and methylation analyses[31]. The elution position on the amide column was smaller than the one of a similar structure, 110.4, which includes Galβ1,4–GlcNAc units in their outer arms[25]. Based on these results, the final form of *N*-glycan digested partially was assigned as 110.4a, and elution positions and suggested structures of digested *N*-glycans A and C are shown in Fig. 8. This indicated that NANA of *N*-glycan A and Fuc of *N*-glycan C was attached to the same α3Man branch of the outer arm and di-HexNAc is GalNAcβ1,4–GlcNAc[31]. The NANA to GalNAc linkage was determined to be α2,6 based on an observed reduction in GU on the amide column[27]. α2,3 NeuAc was reduced to about 0.5 GU on the amide column; on the other hand α2,6 NeuAc increased by about 0.2 GU on the amide column according to the two-dimensional mapping technique[32,33]. The linkage of Fuc in the outer arm of *N*-glycan C was determined to be

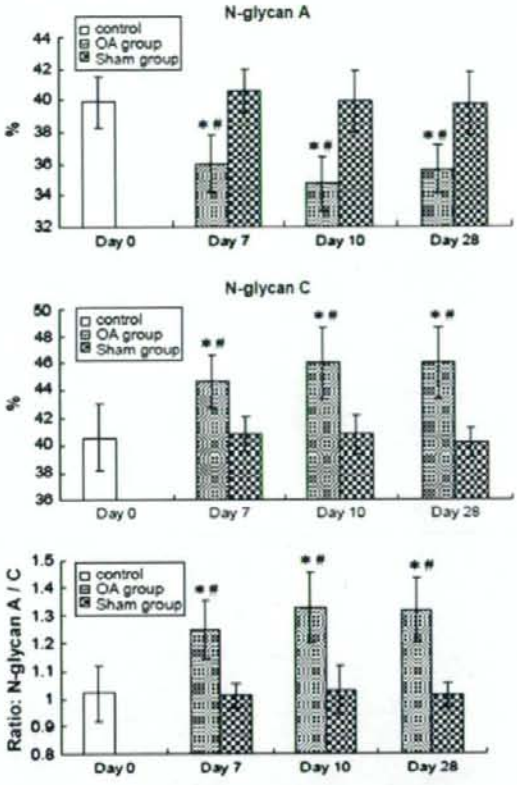

Fig. 5. The ratio in the peak area of *N*-glycans related to OA. Values are means ± SD. The mean ratio of *N*-glycan A decreased significantly from 7 days in the OA group. The mean ratio of *N*-glycan C increased significantly from 7 days in the OA group. The mean ratio of *N*-glycan A–C increased significantly from 7 days in the OA group. *Denotes statistical significance ($P < 0.05$) vs sham group. #Denotes statistical significance ($P < 0.05$) vs control.

an α1,3 linkage to GlcNAc because it was digested with α3/4-Fase and the GalNAc bound to 4 position of GlcNAc. Changing of elution positions with partial digestion is already confirmed in a previous report[32,33]. In this way, structures of *N*-glycans A and C were finally determined as in Fig. 9.

Discussion

The goal of this study was to determine potential alterations in cartilage *N*-glycans with aggravated OA. We first showed alterations in the *N*-glycan peak pattern of articular cartilage between normal rabbit cartilage (sham group) and OA cartilage induced by ACLT (OA group). Then, by comparing peaks obtained from both groups, we showed that the composition of cartilage *N*-glycans was significantly altered in the OA group prior to apparent histological changes. This observation indicates that *N*-glycan alterations in cartilage occur at very early phases of OA aggravation. It is well known that alterations in *N*-glycans are associated with specific disease-related mechanisms[12,13,15]. Several studies of rheumatic diseases report

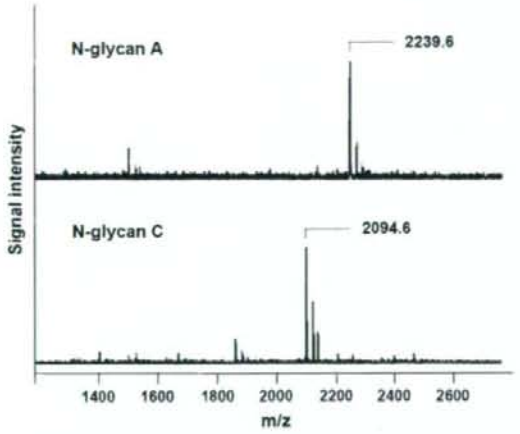

Fig. 6. MALDI-TOF mass spectra. Mass spectrometric analysis of *N*-glycans A and C by the MALDI-TOF/TOF method using DHB as a matrix.

alterations in the *N*-glycan pattern of serum IgG[19–21]. However, little attention has been given to similar alterations in articular cartilage. OA, a chronic degenerative joint disease characterized by articular cartilage deterioration and damage to subchondral bone, is a major cause of disabilities affecting patients' daily activities. Unlike RA, OA is primarily considered a local disease caused by abnormal loading on the articular cartilage. Therefore, analysis of cartilage *N*-glycans may facilitate the understanding of OA pathogenesis. To our knowledge, this is the first study to determine the structure of cartilage *N*-glycans and show alterations in the composition of the cartilage *N*-glycans with OA aggravation.

In early stages of OA aggravation, the macromolecular structure of the ECM is disrupted[5]. Early in this process, chondrocytes begin secreting enzymes that can disrupt ECM macromolecules[1,2]. In particular these enzymes decrease proteoglycan aggregation and concentration of

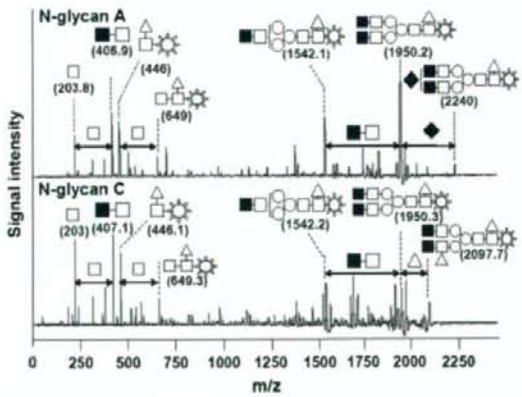

Fig. 7. MALDI-TOF/TOF mass spectra. Structural analysis of *N*-glycans A and C by the MALDI-TOF/TOF method using DHB as a matrix. Structures of fragments of *N*-glycan in each peak are indicated. Mannose, ○; Fuc, △; GalNAc, ■; GlcNAc, □; NANA, ◆; PA, ☼.

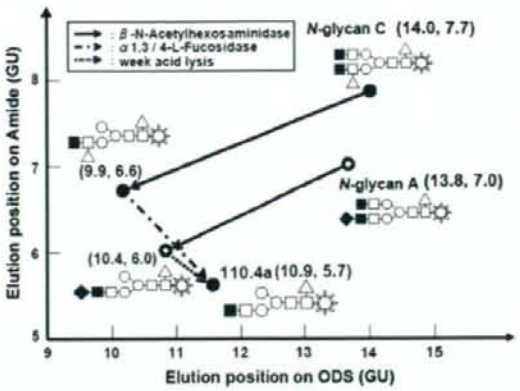

Fig. 8. Structural characterization of *N*-glycans A and C by a combination of exoglycosidase digestion and two-dimensional mapping. A portion of *N*-glycans A and C was digested with exoglycosidases. The elution times on ODS and amide-silica columns of *N*-glycans and their exoglycosidase digests are plotted on a two-dimensional sugar map (expressed as GU). Arrows indicate the direction of changes in the coordinates of *N*-glycans A and C after digestion with: → β-*N*-acetylhexosaminidase, ⇢ α1,3/4-fucosidase, -✦ weak acid lysis.

cartilage ECM, and their release is accompanied by an increased rate of chondrocyte apoptosis in areas of cartilage regeneration. Our analysis indicates that cartilage *N*-glycans undergo changes in the early phases of OA aggravation. *N*-glycans are abundant on the cell surface and in the ECM, and they commonly interact with protein receptors known as lectins. Through this interaction, *N*-glycans mediate cell–cell and cell–ECM interactions and intra- and extracellular signaling. The current study showed alteration in the representation of two kinds of *N*-glycan whose branch has sialic acid and fucose. Although we suppose that these *N*-glycans relate to OA initiation or progression in early phase, their biological functions remain unclear. Further studies will be performed to elucidate their functional roles in OA progression. Therefore, alterations in the composition of 1A1-210.4b (*N*-glycan A) and 210.41b (*N*-glycan C), whose structures are identified here, likely play crucial roles in the response of chondrocytes or

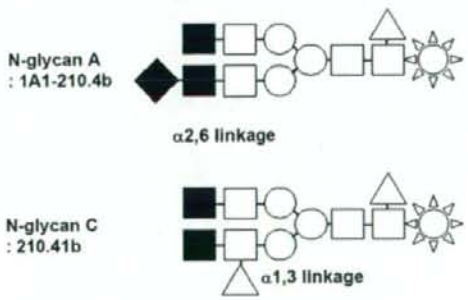

Fig. 9. Structure of *N*-glycans A and C. Indicated are structures of *N*-glycans related to OA. Mannose, ○; Fuc, △; GalNAc, ■; GlcNAc, □; NANA, ◆; PA ☼.

the ECM to changes in the cartilage environment responsible for initiating OA. Here, we did not identify the localization of these *N*-glycans. Future studies are required to determine the biological roles of *N*-glycans identified here in early phases of OA. We observed no significant alterations in the serum *N*-glycan pattern with OA aggravation. Watson *et al.*[20], however, showed alterations in the *N*-glycan pattern of serum IgG with rheumatic diseases, including RA, systemic lupus erythematosus, ankylosing spondylitis, Sjögren's disease, juvenile chronic arthritis, and psoriatic arthritis. In addition to RA, Parekh *et al.*[21] analyzed the *N*-glycan pattern of serum IgG in patients with primary OA and showed that IgG isolated from patients with primary OA contained different distributions of bi-antennary complex-type *N*-glycans. They concluded that primary OA may be a disease related to changes in intracellular processing of *N*-glycans or in their post-secretory degradation. Differences between their results and ours may be due to differences in the *N*-glycan source, to serum or purified IgG, or to mechanisms that induce OA disease. Our current model is a secondary OA model, in which disease is caused by joint instability. Pathological changes must be localized in tissues constituting the joint with cartilage deterioration. Therefore, we conclude that alterations in the *N*-glycan pattern occur in cartilage, not in serum. The results obtained from analysis of both serum and cartilage confirm that OA aggravation following joint instability mainly results from local pathogenesis.

These results and analytical methods can now be applied to clinical studies. The *N*-glycan pattern of articular cartilage may be used as a diagnostic indicator of OA or a predictable indicator of disease aggravation. Although we focus on early phases of OA aggravation, the *N*-glycan pattern of articular cartilage obtained from rheumatic diseases and at advanced stages of OA should now be addressed. By comparing these results, the utility of the *N*-glycan pattern as disease indicators will be established. Also, it is likely that 1A1-210.4b (*N*-glycan A) and 210.41b (*N*-glycan C) identified here play crucial roles in regulating cartilage deterioration following joint instability, but the localization and functional roles of these *N*-glycans are unknown. We are now determining the identities of proteins with specific *N*-glycan structures. When that analysis is complete, we will use knock-out or knock-down of either glycosyltransferase genes or the carrying proteins, followed by a functional analysis of *N*-glycans to further analyze their roles in cartilage deterioration. Finally, the *N*-glycan pattern likely depends on species. For this analysis we used rabbit cartilage, but *N*-glycans altered in human OA cartilage may differ from the *N*-glycans identified here. Thus, the *N*-glycan pattern of degenerative articular cartilage in humans will be analyzed in future studies.

Based on results presented here, we predict that *N*-glycans of human cartilage will alter with cartilage deterioration in diseases such as OA and RA. We will likely observe changes in the linkage of saccharides such as sialic acid and fucose, which is attached to the outer arm of *N*-glycan. Complex combinations of glycosyltransferases and glycosidases control *N*-glycan composition. Therefore, further analysis of expression of glycosyltransferases and glycosidases related to cartilage *N*-glycans should lead to elucidation of the pathogenesis of these diseases.

Regarding the biological and biochemical functions of *N*-glycans obtained in this study, we cannot study any further rabbit model. The reason is that DNA sequences of glycosyltransferases and glycosidases related with cartilage *N*-glycans of rabbit are little known. In our future studies, using human cartilages and conditional model mice, we should determine the functional roles of the *N*-glycans. This should lead to a novel strategy for the treatment of OA.

Recent studies suggest that changes in glycosylation, defined as the addition of sugars to proteins and lipids, have a direct role in the etiology of various diseases, including congenital disorders of glycosylation, von Willebrand factor deficiency, rheumatic diseases, cancers, and emphysema[12,13,19,20,28–30]. Regarding joint diseases, ours is the first study to determine the structure of the cartilage *N*-glycans and analyze potential alterations in damaged cartilage and may provide diagnostics and further insight into OA pathogenesis.

Conflict of interest

The authors have no conflict of interest.

Acknowledgments

We thank Ms Satomi Kudo very much for excellent technical assistance.

References

1. Goldring MB. The role of the chondrocyte in osteoarthritis. Arthritis Rheum 2000;43:1916–26.
2. Bluteau G, Conrozier T, Mathieu P, Vignon E, Herbage D, Mallein-Gerin F. Matrix metalloproteinase-1, -3, -13 and aggrecanase-1 and -2 are differentially expressed in experimental osteoarthritis. Biochim Biophys Acta 2001;1526:147–58.
3. Hamerman D. Aging and osteoarthritis: basic mechanism. J Am Geriatr Soc 1993;4:760–70.
4. Quasnichka HL, Anderson-MacKenzie JM, Tarlton JF, Sims TJ, Billingham ME, Bailey AJ. Cruciate ligament laxity and femoral intercondylar notch narrowing in early-stage knee osteoarthritis. Arthritis Rheum 2005;52:3100–9.
5. Malfait AM, Liu RQ, Ijiri K, Komiya S, Tortorella MD. Inhibition of ADAM-TS4 and ADAM-TS5 prevents aggrecan degradation in osteoarthritic cartilage. J Biol Chem 2002;277:22201–8.
6. Dai SM, Shan ZZ, Nakamura H, Masuko-Hongo K, Kato T, Nishioka K, *et al.* Catabolic stress induces features of chondrocyte senescence through overexpression of caveolin 1: possible involvement of caveolin 1-induced down-regulation of articular chondrocytes in the pathogenesis of osteoarthritis. Arthritis Rheum 2006; 54:818–31.
7. Kouri JB, Rojas L, Perez E, Abbud-Lozoya KA. Modifications of Golgi complex in chondrocytes from osteoarthritic (OA) rat cartilage. J Histochem Cytochem 2002;50:1333–40.
8. Bluteau G, Gouttenoire J, Conrozier T, Mathieu P, Vignon E, Richard M, *et al.* Differential gene expression analysis in a rabbit model of osteoarthritis induced by anterior cruciate ligament (ACL) section. Biorheology 2002;39:247–58.
9. Varki A. Biological roles of oligosaccharides: all of the theories are correct. Glycobiology 1993;3:97–130.
10. Wong CH. Protein glycosylation: new challenges and opportunities. J Org Chem 2005;70:4219–25.
11. Kobata A. Structure and function of the sugar chains of glycoprotein. Eur J Biochem 1992;209:483–501.
12. Yamashita K, Ideo H, Ohkura T, Fukushima K, Yuasa I, Ohno K, *et al.* Sugar chains of serum transferrin from patients with carbohydrate deficient glycoprotein syndrome. Evidence of asparagine-N-linked oligosaccharide transfer deficiency. J Biol Chem 1993;268:5783–9.
13. Wang X, Inoue S, Gu J, Miyoshi E, Noda K, Li W, *et al.* Dysregulation of TGF-β1 receptor activation leads to abnormal lung development and emphysema-like phenotype in core fucose-deficient mice. Proc Natl Acad Sci U S A 2005;102:15791–6.
14. Wacker M, Linton D, Hitchen PG, Nita-Lazar M, Haslam SM, North SJ, *et al.* N-linked glycosylation in *Campylobacter jejuni* and its functional transfer into *E. coli*. Science 2002;298:1790–3.
15. Jaeken J, Carchon H. Congenital disorders of glycosylation: the rapidly growing tip of the iceberg. Curr Opin Neurol 2001;14:811–5.
16. Landberg E, Pahlsson P, Lundblad A, Arnetorp A, Jeppsson JO. Carbohydrate composition of serum transferrin isoforms from patients

with high alcohol consumption. Biochem Biophys Res Commun 1995; 210:267–74.
17. Reitter JN, Means RE, Desrosiers RC. A role for carbohydrates in immune evasion in AIDS. Nat Med 1998;4:679–84.
18. Xiping W, Julie MD, Shuyi W, Huxiong H, John CK, Xiaoyun W, *et al.* Antibody neutralization and escape by HIV-1. Nature 2003;422:307–12.
19. Chou CT. Binding of rheumatoid and lupus synovial fluids and sera-derived human IgG rheumatoid factor to degalactosylated IgG. Arch Med Res 2002;33:541–4.
20. Watson M, Rudd PM, Bland M, Dwek RA, Axford JS. Sugar printing rheumatic diseases: a potential method for disease differentiation using immunoglobulin G oligosaccharides. Arthritis Rheum 1999;42: 1682–90.
21. Parekh RB, Dwek RA, Sutton BJ, Fernandes DL, Leung A, Stanworth D, *et al.* Association of rheumatoid arthritis and primary osteoarthritis with changes in the glycosylation pattern of total serum IgG. Nature 1985; 316:452–7.
22. Tiraloche G, Girard C, Chouinard L, Sampalis J, Moquin L, Ionescu M, *et al.* Effect of oral glucosamine on cartilage degradation in a rabbit model of osteoarthritis. Arthritis Rheum 2005;52: 1118–28.
23. Nakagawa H, Kawamura Y, Kato K, Shimada I, Arata Y, Takahashi N. Identification of neutral and sialyl N-linked oligosaccharide structures from human serum glycoproteins using three kinds of high-performance liquid chromatography. Anal Biochem 1995;226:130–8.
24. Hase S, Ikenaka T, Matsushima Y. Structure analyses of oligosaccharides by tagging of the reducing end sugars with a fluorescent compound. Biochem Biophys Res Commun 1978;85:257–63.
25. Tomiya N, Awaya J, Kurono M, Endo S, Arata Y, Takahashi N. Analyses of N-linked oligosaccharides using a two-dimensional mapping technique. Anal Biochem 1988;171:73–90.
26. Kurogochi M, Nishimura S-I. Structural characterization of glycopeptides by matrix-dependent selective fragmentation of MALDI-TOF/TOF tandem mass spectrometry. Anal Chem 2004;76:6097–101.
27. Takahashi N, Nakagawa H, Fujikawa K, Kawamura Y, Tomiya N. Three-dimensional elution mapping of pyridylaminated N-linked neutral and sialyl oligosaccharides. Anal Biochem 1995;226: 139–46.
28. Sakuma K, Fujimoto I, Hitoshi S, Tanaka F, Ikeda T, Tanabe K, *et al.* An *N*-glycan structure correlates with pulmonary metastatic ability of cancer cells. Biochem Biophys Res Commun 2006;340:829–35.
29. Peracaula R, Tabares G, Royle L, Harvey DJ, Dwek RA, Rudd PM, *et al.* Altered glycosylation pattern allows the distinction between prostate-specific antigen (PSA) from normal and tumor origins. Glycobiology 2003;13:457–70.
30. Mohlke KL, Purkayastha AA, Westrick RJ, Smith PL, Petryniak B, Lowe JB, *et al.* Mvwf, a dominant modifier of murine von Willebrand factor, results from altered lineage-specific expression of a glycosyltransferase. Cell 1999;96:111–20.
31. Tomiya N, Awaya J, Kurono M, Hanazawa H, Shimade I, Arata Y, *et al.* Structural elucidation of a variety of GalNAc-containing N-linked oligosaccharides from human urinary kallidinogenase. J Biol Chem 1993;268:113–26.
32. Tomiya N, Takahashi N. Contribution of component monosaccharides to the coordinates of neutral and sialyl pyridylaminated *N*-glycans on a two-dimensional sugar map. Anal Biochem 1998;264: 204–10.
33. Takahashi N, Wada Y, Awaya J, Kurono M, Tomiya N. Two-dimensional elution map of GalNAc-containing N-linked oligosaccharides. Anal Biochem 1993;208:96–109.
34. Takahashi N, Tomiya N. Analysis of N-linked oligosaccharides: application of glycoamidase A. In: Muramatsu T, Takahashi N, Eds. Handbook of endoglycosidases and glycoamidases. Boca Raton: CRC Press; 1992: 199–332.
35. <http://www.glycoanalysis.info/>; 1992.
36. Nakagawa H, Deguchi K. Structural analysis of sialyl *N*-glycan using pyridylamination and chromatography followed by multistage tandem mass spectrometry. In: Fukuda M, Ed. Methods in Enzymology. San Diego: Elsevier 2006;415:87–104.

CE: Swati; /310; Total nos of Pages: 4;

SPECIAL FOCUS

Elbow

Osteochondritis dissecans of the elbow

Norimasa Iwasaki and Akio Minami

ABSTRACT

Purpose of review

Treatment of osteochondritis dissecans remains challenging. Recently, several techniques for resurfacing a cartilaginous lesion with hyaline cartilage have been developed and applied to osteochondritis dissecans lesions. In this review, we mainly focus on the development of surgical management for osteochondritis dissecans of the elbow over the past year.

Recent findings

The surgical strategy for osteochondritis dissecans of the humeral capitellun (capitellar osteochondritis dissecans) has tended to shift from marrow-stimulating techniques to autologous osteochondral grafts as a cartilage-resurfacing technique. Osteochondral grafts for capitellar osteochondritis dissecans provide better outcomes than simple excision. Regarding the postoperative morbidity of the donor knee, no adverse effect on the donor site is found in young athletes with capitellar osteochondritis dissecans. Additionally, arthroscopic surgery for osteochondritis dissecans lesions has been expanded as well as for other elbow disorders. However, there has been no evidence that arthroscopic surgery for osteochondritis dissecans lesions results in any better prognosis for the patient.

Summary

The goal of treatment for capitellar osteochondritis dissecans is to return patients to their previous level of sport activities and to regenerate long-lasting hyaline cartilage tissue to replace cartilaginous lesions. For this treatment goal, an arthroscopic cartilage-resurfacing procedure may be an ideal treatment for capitellar osteochondritis dissecans.

Keywords

arthroscopy, autologous osteochondral graft, capitellum, osteochondritis dissecans

Department of Orthopaedic Surgery, Hokkaido University School of Medicine, Sapporo, Japan

Correspondence to Norimasa Iwasaki, MD, PhD, Department of Orthopaedic Surgery, Hokkaido University School of Medicine, Kita 15, Nishi 7, Kita-Ku, Sapporo 060-8638, Japan

Tel: +81 11 7065937; fax: +81 11 7066054;

e-mail: niwasaki@med.hokudai.ac.jp

1940-7041

INTRODUCTION

Osteochondritis dissecans (OCD) is an idiopathic lesion affecting an articular surface that involves separation of the cartilage and the subchondral bone. The majority of cases affecting the elbow are found on the humeral capitellum. This lesion frequently occurs in baseball players in their early teens. Although the exact cause of this disease is still controversial, most investigators currently agree that OCD of the capitellum (capitellar OCD) is an overuse injury. The repetitive compression and shear forces to the immature capitellum during throwing are considered to be the main causal factor of this disease.

Regarding treatment strategies, previous studies have stated that acceptable results are generally achieved by nonoperative treatment for the early lesions of capitellar OCD.[1] On the contrary, numerous surgical treatments such as fragment removal with or without drilling or curettage, abrasion chondroplasty, reattachment of the fragments, or closed wedge osteotomy of the capitellum have been advocated for treating advanced lesions.[2–5] These procedures, however, have shown the potential to lead to osteoarthritis and poor functional outcomes. The goal of treatment for capitellar OCD in adolescent athletes is not to temporarily improve symptoms, but to prevent the occurrence of osteoarthritis and to allow patients to return to their previous level of sports activities.

Surgical procedures for the treatment of cartilaginous lesions are mainly categorized into two groups, including marrow-stimulating techniques and cartilage-restoring or cartilage-resurfacing techniques. The marrow-stimulating techniques such as drilling, abrasion chondroplasty, or microfracture attempt to promote a healing response by recruiting pluripotent bone marrow mesenchymal cells. The lesions treated with these techniques are repaired with fibrocartilage scar tissue with biochemical and biomechanical properties inferior to those of hyaline cartilage. On the contrary, recent basic studies related to cartilage tissue engineering have spurred great surgical innovations of cartilage-resurfacing techniques. These techniques, including autologous osteochondral grafts, autologous chondrocyte implantations, and tissue-engineered cartilage transplantations, have become a clinical reality and provided for successful treatment of osteochondral defects in the knee and ankle joints.[6–11]

To achieve the treatment goal mentioned above, resurfacing the OCD lesions of the elbow with hyaline cartilage has been performed in the past few years.[12••,13–17] In this review, we will first describe the cause, diagnostic evaluation, and treatments of capitellar OCD, and then review the advances of the past year in the treatment strategies for this lesion.